Simulation of UV photodissociation of $I_2^-(CO_2)_n$: Spin-orbit quenching via solvent mediated electron transfer

N. Delaney, J. Faeder, and R. Parson[a)]
JILA and Department of Chemistry and Biochemistry, University of Colorado and National Institute of Standards and Technology, Boulder, Colorado 80309-0440

(Received 15 February 1999; accepted 16 April 1999)

We simulate the 395 nm photodissociation of I_2^- embedded in clusters of 6 to 22 CO_2 molecules. In the isolated molecule, photodissociation at this wavelength leads exclusively to spin-orbit excited iodine (I^*) plus I^-. In the larger clusters we observe efficient electronic relaxation, leading both to dissociated products containing ground-state iodine and to recombined products containing I_2^-. The time scale and cluster size dependence of the spin-orbit quenching process agree well with experimental determinations of Sanov *et al.* (companion paper). The simulation trajectories show that spin-orbit quenching occurs by resonant charge transfer from solvated I^- to a nascent I^* atom. A model derived from the theory of electron transfer reactions in solution illustrates that this resonance arises when the I spin-orbit energy is compensated by the difference between the solvation energies of the ion and the neutral. © *1999 American Institute of Physics.* [S0021-9606(99)01626-8]

I. INTRODUCTION

In the decade that has passed since the pioneering experiments of Lineberger and co-workers,[1,2] dihalide ions have become favorite models for studying the effects of strong solvent-solute forces on elementary chemical reactions. In particular, I_2^- has been studied in a wide variety of environments, including gas phase clusters,[3–12] liquid solutions,[13–21] and gas-surface collisions,[22–25] and these experiments have stimulated a variety of theoretical studies.[26–47] These solvated molecular ions differ considerably from their neutral counterparts, since the interaction between the ion and the surrounding solvent, which can be as strong as the chemical bonding forces within the solute, depends sensitively on the solute charge distribution. The electronic structure of the solvated ion is subject to strong perturbations that depend on the coordinates of the solvent molecules. Therefore, the dynamics takes place on multidimensional potential energy surfaces that cannot be represented in terms of pairwise interactions at even the lowest level of approximation. We are confronted by two sorts of challenges: to develop an accurate method for simulating dynamics on these surfaces, and to devise a conceptual picture with which to interpret the results of these simulations and to predict the results of future experiments.

Within the past two years the technical challenge has been met through the development of effective Hamiltonian descriptions of the electronic structure of the interacting solute-solvent system.[41–46] Nonadiabatic molecular dynamics simulations computed with these Hamiltonians have successfully reproduced the results of both time-independent and time-dependent experiments. The results of these simulations demonstrate that physical pictures based on the isolated molecule potential curves can be highly misleading. For example, the gas phase photodissociation of I_2^- at 790 nm takes place directly on the repulsive A' state (Fig. 1); however, both simulations[43,46] and experiment[11] show that in a cluster of CO_2 molecules this channel is closed and that dissociation only occurs via nonadiabatic transitions to the lower A and X states.

In recent papers[43,45] we have attempted to meet the conceptual challenge by developing a pictorial representation inspired by the theory of electron transfer reactions in solution.[48–50] The underlying idea is that crucial aspects of the dynamics are determined by the competition between solvation forces, which tend to localize the solute charge distribution on a single atom, and chemical bonding forces, which prefer a delocalized molecular charge distribution. This motivates us to interpret the solvent dynamics in terms of a collective ''solvent coordinate,'' defined in terms of the electrostatic potential that the solvent exerts at the two solute atoms. This coordinate describes the energetic asymmetry of the local solvent environment; the competition between solvation and chemical bonding can be illustrated by plotting the simulation trajectories as a function of the solute bond length and of this solvent asymmetry coordinate. The clear and simple patterns displayed when the dynamics is presented this way help untangle the dynamics of solvent-induced nonadiabatic transitions.

In this paper we present results of the simulation of the photodissociation of I_2^- following excitation at 395 nm, which brings the solute to states that correlate, in the isolated molecule, to a spin-orbit excited iodine atom (I^*) and an I^- ion, and extend the conceptual framework outlined above to aid in interpreting these dynamics. We describe an efficient mechanism for quenching the spin-orbit excited states when the molecule is embedded in a cluster. This mechanism, first suggested during our earlier study of I_2^- in a uniform electric field,[36] involves charge transfer from a nascent solvated I^- ion to the I^* atom, yielding I^- and solvated I in its spin-orbit ground state. The 0.94 eV energy gap between I and I^* is

a)Author to whom correspondence should be addressed; electronic mail: rparson@jila.colorado.edu

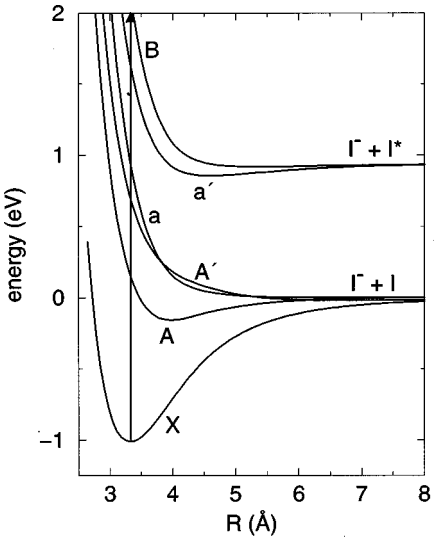

FIG. 1. Scaled *ab initio* gas phase potential curves for I_2^-. The arrow shows the 395 nm photoexcitation to the $B\ ^2\Sigma_{g,1/2}^+$ state modeled in the current simulations.

compensated by the difference between the ion and neutral solvation energies. The molecular dynamics simulations demonstrate that spin-orbit quenching is indeed efficient, and analysis of the simulations using the electron-transfer picture confirms the proposed mechanism. In a companion paper, Sanov *et al.* provide convincing experimental evidence for the process as well.[51] Both simulation and experiment find that the time scale for electronic relaxation is a few picoseconds, orders of magnitude faster than observed for the collisional quenching of I* by CO_2[52] or the electronic relaxation of I* pairs in liquids and in solid matrices.[53,54]

The paper is organized as follows. Section II gives a brief overview of the simulation methods; a complete discussion may be found in Refs. 44 and 45. The products of the trajectory simulations are described in Sec. III. Section IV focuses on the dynamics we observe in a range of cluster sizes around half a solvation shell ($n=6-13$), highlighting the onset of spin-orbit relaxation. Section IV A describes the effects of solvation on the electronic states of I_2^-, and forms the framework for our discussion of the dynamics. (In the Appendix, these ideas are illustrated in more detail using a simple one-electron Hamiltonian analogous to those used in the theory of electron transfer.) Details of the initial photofragmentation process are presented in Sec. IV B, and support for the proposed solvent-mediated relaxation of I*is given in Sec. IV C. The dynamics is summarized in Sec. IV D, and Sec. V concludes the paper.

II. METHODS

The simulations described here use the same effective Hamiltonian model as our earlier studies of photodissociation dynamics at 790 nm.[43,45] While in the earlier studies the electronic states that correlate to spin-orbit excited iodine were not populated, they were included in the basis states of the Hamiltonian, so no significant changes are required to apply the model to UV photodissociation. The interaction between the solute I_2^- and the solvent CO_2 molecules is described by an operator that includes state-dependent electrostatic and induction interactions between the solute and solvent based on *ab initio* calculations of the solute wave functions[55] and experimental data for the solvent charge distribution[56] and polarizability.[57] The one-electron density matrix derived from the solute wave functions is expanded in distributed multipole operators;[58] diagonal elements of the distributed multipoles describe the solute charge density in various electronic states, while off-diagonal elements describe transition charge densities that allow for polarization of the solute charge density by the solvent. State-independent atom-atom Lennard-Jones potentials account for the remaining dispersion and repulsion interactions; these are fit to reproduce the known $I^- - CO_2$ and $I - CO_2$ potential curves.[59] The $CO_2 - CO_2$ interaction potential is taken from Murthy *et al.*[56] This model captures the sensitive dependence of the solute charge distribution on the solute electronic state, the solute bond length, and the positions and orientations of the solvent molecules.

At each time step the matrix of the effective Hamiltonian, which depends parametrically upon the coordinates of all the solute and solvent nuclei, is constructed and diagonalized, yielding the energies, forces, and nonadiabatic transition matrix elements required to proceed to the next step; distributed multipole analysis allows us to derive compact analytical expressions for these quantities.[45] Nuclear motion on a single potential surface is computed using the velocity version of the Verlet algorithm,[60] while hopping between surfaces is computed using Tully's method[61,62] with some minor modifications to account for nuclear decoherence.[42,45] Since the trajectories are integrated in the adiabatic representation, phenomena such as charge transfer do not necessarily involve a transition between states, but can instead take place adiabatically as a trajectory moves through an avoided crossing region.

For each cluster size studied, 100 trajectories were computed from starting configurations obtained by sampling a single 1 ns trajectory with an average temperature of 80 K. This temperature was chosen to lie on the upper end of the solid-liquid phase transition region in the clusters, based on our previous experience that such temperatures gave reasonable agreement with experimental results[42] (the experimental cluster temperatures are known only very approximately[63]). The products are determined by integrating the trajectories until the nuclear configuration meets either of two criteria: the I–I distance exceeds 40 Bohr, or I_2^- undergoes more than 25 oscillations in a particular potential well. The dissociation and recombination times vary from a couple of picoseconds to over 100 ps in some cases where I_2^- is temporarily trapped in an excited electronic state. The time scale for evaporation of CO_2 molecules from the clusters following photodissociation appears to be much longer than the 2–100 ps over which the trajectories are integrated, and thus our mass distributions are expected to be shifted to larger mass with respect to the experimental results, which are measured at 5–10 μs.[3,64]

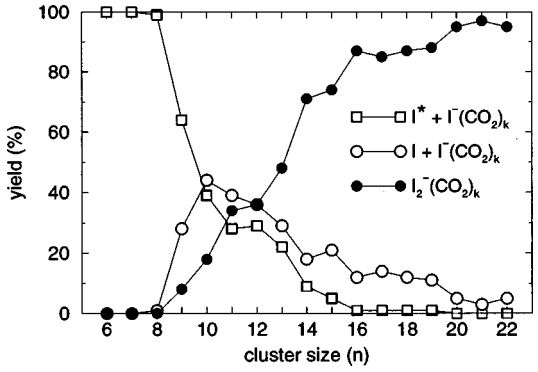

FIG. 2. Branching ratios for the products of $I_2^-(CO_2)_n$ photodissociation at 395 nm. $1\sigma = \pm 5\%$.

III. PHOTOFRAGMENTATION PRODUCT DISTRIBUTIONS

The fragments resulting from photodissociation of $I_2^-(CO_2)_n$ at 395 nm can be grouped into three product channels, two of which correspond to a dissociated solute ($I^- + I$) and one to a recombined solute (I_2^-). The two dissociative channels differ in the average number of CO_2 molecules left surrounding the I^- fragment. As discussed in the companion paper,[51] this difference is energetically consistent with the amount of CO_2 evaporation that is expected to follow internal conversion of the iodine spin-orbit energy into solvent motion, and our simulations allow us to confirm that the heavy I^--based fragments result from dissociation on the a' excited spin-orbit state (see state labels, Fig. 1), whereas both the light I^--based fragments and the recombined fragments require relaxation to the lower spin-orbit states of I_2^-. The relative intensity of each product channel as a function of the initial cluster size is shown in Fig. 2.

Figure 3 shows the mass distribution of products from simulated photodissociation of $I_2^-(CO_2)_n$ for selected cluster sizes at 395 nm. We expect our distributions to be shifted to larger mass relative to the experimental distributions since the trajectories are terminated before solvent evaporation is complete. For cluster sizes $n \leqslant 7$ we see a single mode of I^--based products centered at about $k = n - 3$, corresponding to dissociation to solvated $I^- + I^*$. At $n = 8$, there is essentially still a single mode of dissociative products; however, 2% of the trajectories undergo spin-orbit relaxation before dissociating. For $n = 9$, about 35% of the trajectories are spin-orbit quenched, and there is a distinct second peak in the mass distribution of I^--based products corresponding to the loss of 3–4 additional CO_2 molecules. Also, we begin to see recombined I_2^- products. This sharp onset of spin-orbit relaxation is discussed in Sec. IV. By $n = 11$ the three product channels are roughly equal in intensity, and as the cluster size increases ground-state recombination becomes the dominant product. By $n = 20$, dissociation to $I^- + I^*$ is no longer observed, but dissociation on the lower spin-orbit states is not completely quenched at $n = 22$, the largest cluster size studied.

These trends are in broad agreement with the experimental observations of Sanov *et al.*, although there are significant differences in detail. In particular, we do not see the finely

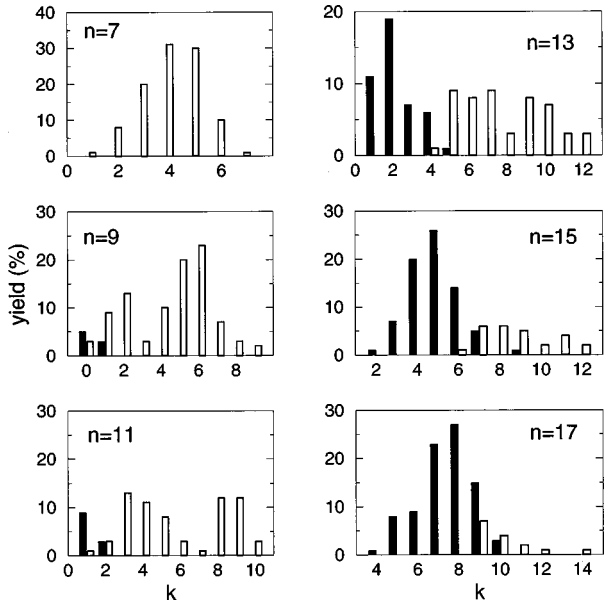

FIG. 3. Simulated mass distribution of products for selected cluster sizes. Open bars represent I^--based products, filled bars represent I_2^--based products. The high mass dissociative fragments are produced in conjunction with I*, while the low mass fragments are accompanied by I in its ground spin-orbit state.

structured dependence of the caging fraction on cluster size that is reported experimentally. Nor do we see the recombination channel opening at smaller cluster sizes than dissociation from the lower spin-orbit states. Finally, the simulations overestimate the caging fraction for intermediate and large cluster sizes. These discrepancies contrast with our earlier simulation of 790 nm photodissociation,[43] where quantitative agreement with experimental branching ratios was achieved, and suggest that ultraviolet (UV) photodissociation provides a more sensitive test of the simulation model. Nevertheless, the simulations and experiments deliver the same overall message: spin-orbit quenching, which is completely absent in the isolated molecule and in the smaller clusters, suddenly becomes efficient in clusters having more than 7–8 CO_2 molecules.

IV. DYNAMICS

A. Qualitative picture of solvent-mediated electronic relaxation

The photofragmentation process is driven by the interaction between the solvent molecules and the changing charge distribution of I_2^- in its various electronic states. Since the electronic structure of the solute is strongly perturbed by the solvent, it is often misleading to interpret the dynamics in terms of the potential curves of isolated I_2^- alone.[43] In the present case, the most interesting features of the relaxation dynamics take place at solute bond lengths of 5–10 Å, where the potential energy curves of isolated I_2^-, shown in Fig. 1, are nearly flat. Under these circumstances the dynamics is dominated by motions within the solvent. A similar situation arises in the theory of electron transfer in solutions,[48–50] where the ''reaction coordinate'' consists of solvent reorganization, and in previous work we have used a schematic

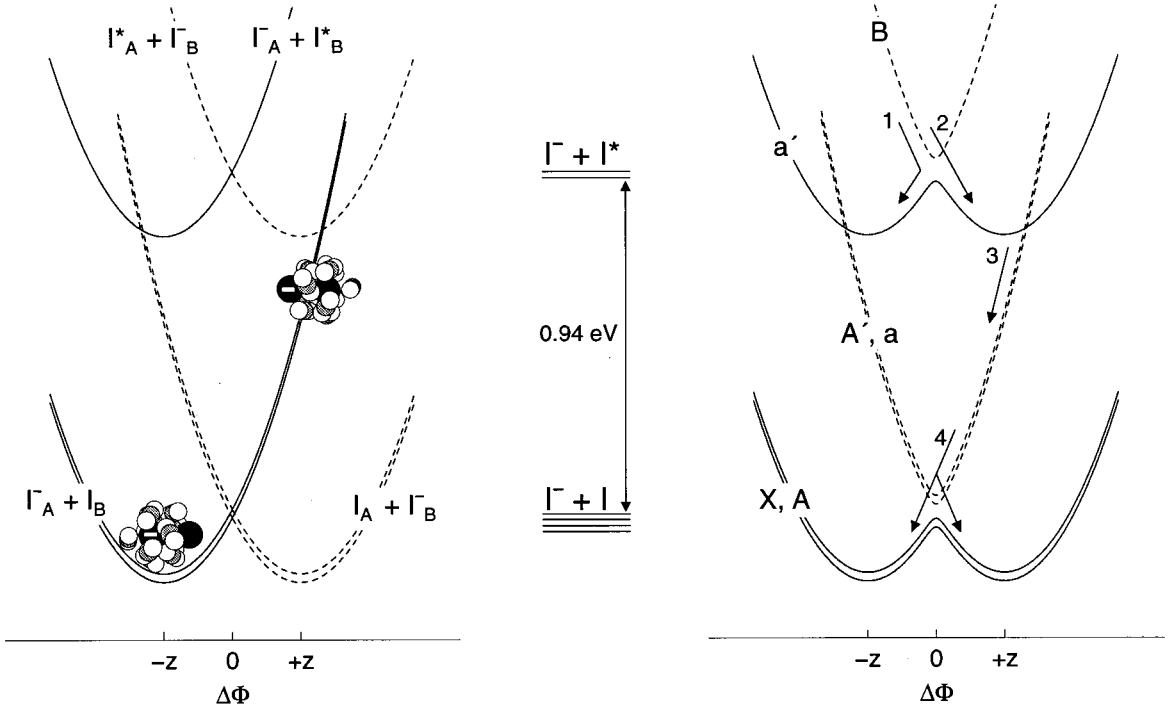

FIG. 4. Solvation effects on the solute potential energy at intermediate to large solute bond lengths. Center: energy levels of isolated $I^- + I$ in its two lowest electronic states. Left-hand panel: diabatic energy vs solvent coordinate, $\Delta\Phi$. Right-hand panel: adiabatic states associated with molecular state labels of I_2^-. States B, A', and a exhibit anomalous charge flow. Arrows depict relaxation pathways observed in trajectories.

picture inspired by the classical Marcus theory[48] to interpret the photofragmentation process following excitation at 790 nm. Here we extend this picture to include the states that correlate to spin-orbit excited iodine. With this model to guide the analysis of our simulations, we demonstrate that the mechanism for spin-orbit relaxation of I_2^- inside the cluster is a form of solvent-induced charge transfer. In the Appendix we examine these ideas in more depth using a simple one-electron model Hamiltonian. We emphasize that these simple models are used to only interpret the simulation results, not to calculate them. As described in Sec. II, the simulations use an effective Hamiltonian that explicitly includes all of the solvent molecules and an accurate representation of the solute charge distribution based on a distributed multipole analysis of the *ab initio* wave functions.

Figure 4 displays the electronic energy levels of I_2^- at large internuclear distances where both the spin-orbit energy and the ion solvation energy exceed the chemical bonding interaction between I and I^-. The center panel shows the energy levels of the isolated solute. The two upper states correlate to $I^- + I^*$, while the four lower states represent $I^- + I$; these levels are separated by the atomic spin-orbit splitting of 0.94 eV. The remaining panels in the figure show how these energy levels are influenced by the solvent. For this purpose we introduce a collective coordinate that describes the asymmetry of the local environment around the solute. The ''solvent coordinate'' is defined as the electrostatic potential difference between the two I atoms, i.e., the difference in energy when a charge of $-e$ is moved from I_A to I_B holding all nuclear coordinates fixed. The magnitude of the solvent coordinate, $\Delta\Phi$, is small when the solvent molecules are nearly equally shared between the two iodine nuclei (a ''symmetric'' cluster) and large when one nucleus is preferentially solvated (an ''asymmetric'' cluster).

In the left-hand panel we adopt a diabatic picture in which the $I\cdots I^-$ resonance coupling is neglected. The energy of the solute-solvent system is minimized when the ion charge is localized on a single atom and the solvent surrounds that atom. Since the charge may reside on either iodine atom, this leads to two equivalent minima when the energy is plotted against the solvent coordinate; these minima are located in the figure at $\Delta\Phi = \pm z$. Associated with each minimum is a diabatic potential curve which, to a first approximation, depends quadratically on the solvent asymmetry coordinate; motion along this ''Marcus parabola'' entails reorganizing the solvent cluster while holding the electronic charge distribution fixed. For example, the minimum at $-z$ corresponds to solvated $I_A^- + I_B$, and as the system moves along the diabatic curve toward larger values of $\Delta\Phi$ the cluster becomes more symmetric, which raises the electronic energy since the solvent molecules are on average farther away from the solute charge. When the solvent coordinate has reached a value of $+z$, the solvent has moved all the way from I_A^- to I_B, incurring a large energetic penalty, and at sufficiently large solvent coordinates the solvation energy exceeds the spin-orbit splitting energy so that the diabatic states of ground-state iodine cross those associated with

I*. At zero solvent coordinate, the symmetrically equivalent pairs of diabatic states intersect and the degeneracy pattern of isolated I_2^- is recovered. The actual solvent motions involved in this problem are different from those invoked in the usual Marcus picture. In classical Marcus theory, solvent reorganization is brought about by reorientation of the dipolar solvent molecules, whereas here the solvent cage moves from one side of the solute to the other. Thus the solvent coordinate can be very large in these systems even though our solvent molecules have no permanent dipole moments.

In the right-hand panel we restore the electronic coupling to a value corresponding to a solute bond length of 7–10 Å. The crossings at zero solvent coordinate become avoided crossings, and we can attach the molecular state labels of I_2^- to the resulting curves.[65] A comparison to the diabatic curves in the left-hand panel illustrates the two types of charge flow that we have identified in these systems. At the point $-z$ on the A or X state the charge is localized on I_A and the solvent favors this end of the diatom. Moving toward a solvent coordinate of $+z$ along the lower adiabatic curve, the solute charge and the solvent environment reorganize in concert, crossing a barrier at $\Delta\Phi=0$ and resulting in I_A+solvated I_B^-; we have called this ''normal charge flow.'' In contrast, a vertical excitation from the system at point $-z$ on the A or X state to the antibonding A' or a state corresponds to shifting the balance of charge from I_A to I_B while the solvent remains near I_A. As the solvent migrates away from I_A, toward the excess charge, the solute electronic energy rapidly decreases. However, after crossing the zero solvent coordinate, the electronic character of the state changes to $I_A^- + I_B$, and the solvent is once again on the uncharged end of the solute. Thus during adiabatic motion on the upper curve, the solute charge and the solvent environment move in opposition to each other; we have called this ''anomalous charge flow.''[36,37,42,43,45] The same dichotomy applies to the two states of the upper spin-orbit manifold: charge flow is normal on the a' state and anomalous on the B state.[36] This illustration of the origin of normal and anomalous charge flow states is complementary to the explanation we gave in Ref. 45, Sec. 5. In a simple diatomic linear combination of atomic orbitals-molecular orbitals (LCAO)-(MO) picture of I_2^-, the atomic orbitals of I^- and I combine to produce delocalized bonding and antibonding molecular orbitals. An asymmetric solvent environment polarizes the solute charge distribution in the bonding state so that the excess charge resides mostly on the more solvated atom. Since the ground and excited states must remain orthogonal, the charge localizes on the less solvated atom in the antibonding state. In general, states that are predominantly bonding in character exhibit normal charge flow, while states that are predominantly antibonding in character exhibit anomalous charge flow. The validity of this description for charge flow in these systems is demonstrated by the good agreement between the experimental and simulated photodissociation products of $I_2^-Ar_n$ clusters.[42] The key distinction between states with normal and anomalous charge flow is the location of the energy minimum along the solvent coordinate. States showing anomalous charge flow funnel the system toward symmetric cluster configurations, while states showing normal charge flow favor an asymmetric cluster environment.

With the aid of Fig. 4, we can identify the types of electronic transitions and the relaxation pathways observed in our system. An excitation of 395 nm takes the system to the B state, and transitions to the a' state occur when the solvent coordinate is nearly zero. A simple diabatic passage through this region corresponds to solvent transfer, in which the solvent cage moves from one side of the solute to the other while the electronic charge distribution is unchanged. This is indicated by arrow 2 on Fig. 4. If, however, the excess charge is transferred from one iodine atom to the other as the system moves through the coupling region, the solvent returns to the side on which it began, as illustrated by arrow 1. In this respect, the short-time dynamics on the B state following UV excitation resemble those observed on the A' state following visible excitation.[45,46] Once on the a' state, however, the system may hop to the A' or a state at the points of intersection with the a' curve, arrow 3. This charge transfer differs from transitions seen in our 790 nm simulations, in that it occurs only from highly asymmetric solvent configurations. Following this charge transfer to the lower spin-orbit states, reorganization and evaporation of solvent molecules dissipate the excess potential energy and return the system to the coupling region between the a/A' and A/X states, where both solvent and charge-transfer transitions take place, shown by arrow 4. Sections IV B and IV C describe the results of our nonadiabatic dynamics simulations within this framework.

B. Early times: Spin-orbit excited states

Before photoexcitation, the solute is at equilibrium in its ground (X) electronic state, where the I_2^- bond is stable relative to the solute-solvent interactions of roughly 200 meV per CO_2 molecule. Clusters in the size range $n=6$–13, on which we focus this discussion, contain approximately half a solvation shell of CO_2 molecules, which group together about one end of I_2^-, producing an asymmetric solvent environment.[27,37,43,46]

At $t=0$, the solute is promoted to the repulsive B state. The excess charge flows rapidly to the less solvated iodine atom, and the solvent responds to this change in the solute polarization on a time scale of a few hundred femtoseconds. The I_2^- bond length increases to 5 Å in roughly 150 fs, before translational motion of the solvent molecules begins. As R_{solute} increases, the charge becomes fully localized on the less solvated iodine and moves farther away from the solvent. The Coulombic attraction between I^- and the CO_2 cluster slows and ultimately prevents dissociation on the B state.[66] The CO_2 molecules continue to move toward the charge, though, making the solvent environment more symmetric. By this point the solute bond length is sufficiently extended that the a' and B electronic states become degenerate as the solvent coordinate approaches and passes through zero, and nonadiabatic transitions begin to take place. Figure 5 shows the population of the B and a' electronic states versus time for selected cluster sizes. For all cluster sizes studied, trajectories begin hopping to the a'

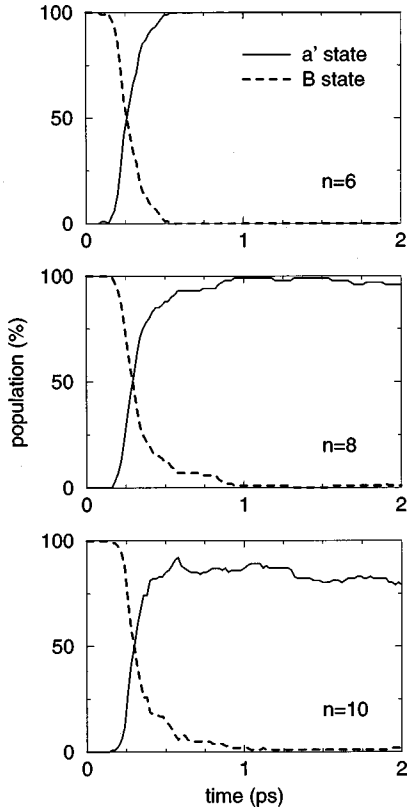

FIG. 5. B and a' electronic state populations vs time, $n=6,8,10$. The tail in the B state population is evident in cluster sizes $n=8,9,10$ and to a lesser degree at $n=11$. A similar lengthening of the time for electronic relaxation from the A' state was observed in our simulations of photodissociation at 790 nm and was attributed to the time required for solvent rearrangement to occur in asymmetric clusters.

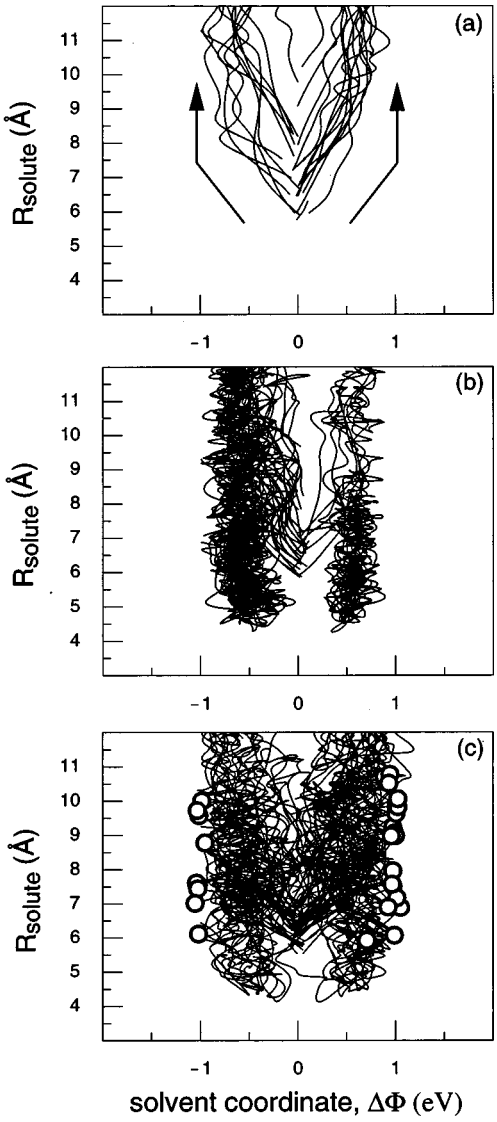

FIG. 6. Motion on the a' state for selected trajectories with $n=8$ (a), (b) and $n=9$ (c). (a) Trajectories producing heavy fragments (six or seven solvent molecules remain) dissociate directly on the a' state. (b) Trajectories producing fragments with four solvent molecules predominantly undergo transient trapping on the a' state before dissociating. (c) Trajectories that relax to the lower spin-orbit states. The transitions, marked by the circles, occur near $\Delta\Phi=\pm 1$ eV, just beyond the solvent coordinates accessed in $n=8$ trajectories.

state at about 200 fs, and most have made the transition by 500 fs. Once on the a' state, the solvent can catch I^- and dissociation can proceed. For clusters with seven or fewer CO_2 molecules, R_{solute} increases monotonically following transition to the a' state, producing solvated I^- and I*; we refer to this as direct dissociation. The average times required to reach an I^*-I^- separation of 40 Bohr ($\approx$20 Å) are 1.9 and 3.7 ps for $n=6$ and 7, respectively.

Although direct dissociation accounts for some of the products in larger cluster sizes, other mechanisms become possible with increased solvation. For $n=8$, where a single product mode is observed in the mass distribution, two types of trajectories are observed. The products with five or more CO_2 molecules are formed by direct dissociation on a time scale of about 5 ps, while the trajectories leading to products with four or fewer solvent molecules require about 19 ps. The origin of this difference in time scale is illustrated in Fig. 6, which maps out the motion of the trajectories on the a' state as a function of R_{solute}, the I_2^- bond length, and $\Delta\Phi$, the solvent coordinate. All trajectories enter the a' state at $\Delta\Phi\approx 0$. The trajectories producing heavy fragments dissociate promptly on the a' state, Fig. 6(a), while trajectories with lighter products are characterized by diffusive motion on the a' state, which delays dissociation until I* escapes via thermal evaporation, Fig. 6(b). A similar trapping event occurs on the A state following 790 nm excitation of I_2^- in CO_2 clusters.[43,45,67]

For $n=9$, the I^-+I^* products that retain 6–9 solvent molecules form in 1–5 ps. Most of the remaining trajectories are trapped for some period of time on the a' state, but the additional CO_2 molecule allows many trajectories to reach large values of the solvent coordinate where relaxation to the lower spin-orbit manifold takes place. Figure 6(c) shows the location of transitions from the a' to the a and A' states. Of the trajectories that relax to the lower manifold, most dissociate to I^-+I in an average time of 19 ps, with three or fewer CO_2 molecules bound to the final I^- product, while others recombine as discussed below. Trajectories trapped in the a' state that do not undergo nonadiabatic transitions dissociate to $I^-(CO_2)_{4,5}+I^*$ in about 15 ps.

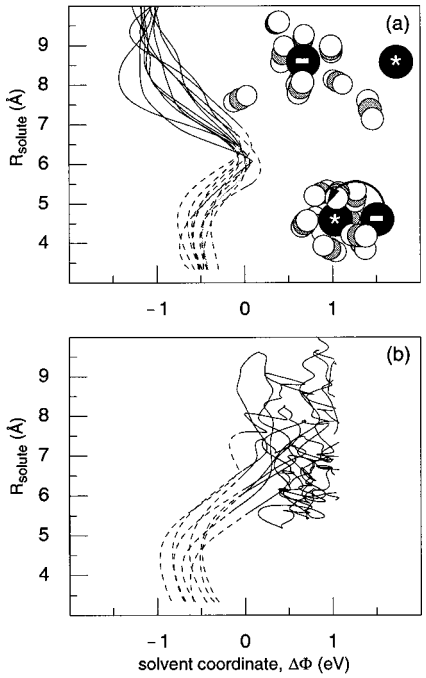

FIG. 7. Motion on the B and a' states for selected trajectories with $n=11$. Trajectories begin at $R_{solute}=3.3$ Å on the B state (dashed lines) and transfer to the a' state (solid lines) near $\Delta\Phi=0$, $R_{solute}=5-8$ Å . (a) Charge transfer followed by direct dissociation, producing heavy I^- fragments. (b) Solvent transfer followed by transient trapping on the a' state.

For the intermediate cluster sizes, $n=9-12$, another distinction between the rapidly dissociating and trapped trajectories becomes apparent in the early-time dynamics. As discussed in the previous section and illustrated in Fig. 4(c), there are two ways to make a nonadiabatic transition from the B state to the a' state: charge transfer and solvent transfer. Either the excess charge can transfer from the unsolvated to the solvated iodine atom, or the solvent can migrate to the charged iodine; these pathways are depicted by arrows 1 and 2, in Fig. 4(c), respectively. For trajectories that begin with a near-zero solvent coordinate it can be difficult to separate the charge and solvent motions, but for clusters with about half a solvent shell the distinction is clear. Figure 7 traces the paths of several trajectories in the $n=11$ ensemble from excitation through the $B\rightarrow a'$ transition and the subsequent motion on the a' state. For ease of illustration, the trajectories shown all begin as solvated $I_A^*+I_B^-$, but the overall picture is symmetric under reflection through $\Delta\Phi=0$. As the solute dissociates on the B state, the attempted motion of I_B^- away from the solvent cluster slows the dissociation, providing time for the solvent to reorganize enough to bring about coupling between the B and a' states. In trajectories that undergo charge transfer, shown in Fig. 7(a), the charge hops, forming solvated I_A^-, and I_B^* escapes. Figure 7(b) shows trajectories crossing $\Delta\Phi=0$ as the transfer of CO_2 molecules yields I_A^* + solvated I_B^-, trapped on the a' state. Table I shows that for intermediate cluster sizes, charge transfer from B to a' primarily results in fast dissociation on the upper spin-orbit states, while solvent transfer usually precedes spin-orbit relaxation. The following section further details the role of solvent motion in inducing relaxation to the lower spin-orbit manifold.

TABLE I. Correlation of $B\rightarrow a'$ transition type with final products. The percentage of trajectories, normalized within each product channel, that undergo charge transfer (CT) or solvent transfer (ST).

n	I^-+I^* % CT	I^-+I % ST	I_2^- % ST
10	68	95	100
11	90	75	88
12	89	91	78

C. Later times: Spin-orbit relaxation and recombination

When the I_2^- solute is in its a' electronic state, asymmetric cluster configurations are favored. Figure 4(c) shows that increasing solvation destabilizes the a and A' electronic states, which cross the a' state at a large value of the solvent coordinate. This crossing occurs when the asymmetric solvent environment compensates for the energy gap between these electronic states in bare I_2^-, which at $R_{solute}>5$ Å is essentially the spin-orbit splitting of iodine atom, 0.94 eV. This type of mechanism was suggested, in a more speculative context, in an earlier study of the electronic structure of I_2^- in a uniform electric field;[36] there it was referred to as ''field-induced resonance.'' In our trajectories, transitions to the lower spin-orbit manifold occur at solvent coordinates greater than 0.75 eV. Since $n=9$ is the smallest cluster size for which such values are commonly reached on the a' state (see Fig. 6), this marks the onset of appreciable spin-orbit relaxation in our simulations.

Figure 4 also demonstrates that a transition from the a' state to either the a or A' state involves transferring an electron between the two iodine atoms. Since electron transfer requires nonzero overlap of the wave functions on the two iodine atoms and therefore cannot occur over an arbitrarily large distance, spin-orbit relaxation is not seen in the most rapidly dissociating clusters. Trajectories that reach solvent coordinates of about 1 eV before R_{solute} exceeds about 10 Å have an opportunity to relax. If R_{solute} is larger, the a' state simply becomes lower in energy than the a and A' states, no transition occurs, and I_2^- dissociates to I^-+I^*.

If the charge-transfer transition does occur, the solvent suddenly finds itself far out of equilibrium with the solute charge distribution, having acquired about 1 eV of excess potential energy. Since much of this is immediately converted to kinetic energy, the cluster virtually explodes. Some trajectories dissociate directly on the a and A' anomalous charge switching states, an event not observed in 790 nm excitation except in the smallest clusters. However, the majority of trajectories make transitions to the A and X states from the A' or a state minimum at $\Delta\Phi=0$. These transitions occur by either charge or solvent transfer, and the two are difficult to distinguish, because the solvent coordinate remains small. If the escaping solvent molecules remove enough energy, the I_2^- bond can reform on the X state and undergo vibrational relaxation. Although we have not ana-

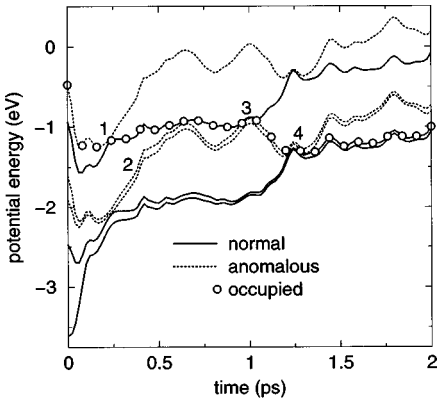

FIG. 8. Cluster potential energy of each electronic state vs time for a single trajectory. Initially, the states are, in order of increasing energy, *X*, *A*, *A′*, *a*, *a′*, *B*. 1. Transition from state *B* to state *a′*. 2. Solvent reorganization, increasing cluster asymmetry, is implied by the destabilization of anomalous charge flow states. 3. Spin-orbit relaxation via charge-transfer transition from state *a′* to state *a* followed by solvent reorganization. 4. Transition from state *a* to state *A*. For this trajectory, I_2^- ultimately dissociates on the *A* state (not shown).

lyzed the final vibrational relaxation completely, we find it to be much slower than observed in 790 nm dissociation, as far fewer solvent molecules remain to dissipate energy.

Figure 8 shows the potential energy of the cluster in each electronic state as a trajectory progresses. To conserve space, a trajectory with faster than average relaxation dynamics is shown. States of the same charge switching character run roughly parallel to each other, since they respond similarly to changes in the solvent environment. At 250 fs this trajectory makes a $B \rightarrow a'$ transition. As the cluster reorganizes to a larger solvent coordinate on the a' state between 250 and 500 fs, the anomalous charge flow states are *destabilized*. At 1 ps the trajectory undergoes charge transfer to the *a* state, followed by a rapid reorganization of the solvent, which stabilizes the anomalous charge switching states and brings the four states of the lower spin-orbit manifold into resonance. There the trajectory hops to the *A* state at 1.25 ps and I_2^- dissociates.

Figure 9(a) displays the ensemble average of the magnitude of the solvent coordinate as a function of time for $I_2^-(CO_2)_{13}$. The ensemble is divided according to the three types of final products. Figures 9(b) and 9(c) show the electronic state populations vs time for the same ensemble, with the trajectories that dissociate on the a' state omitted. Figure 9(b) shows the populations of the *B* and a' states, and Fig. 9(c) shows the population of states in the ground spin-orbit manifold grouped by charge flow character. Following excitation to the *B* state, all trajectories experience a slight increase in the solvent coordinate due to the increase in the I_2^- bond length. However, immediately afterward the solvent coordinate decreases sharply as anticipated for the anomalous *B* state [inset, Fig. 9(a)]. The sharp rise at 200 fs coincides with hopping to the a' state, where large solvent coordinates are favored. From this point the $I^- + I^*$ products dissociate directly with the solvent coordinate increasing with R_{solute} until it reaches a maximum value. Meanwhile, between 0.5 and 3 ps the remaining trajectories begin making transitions to the *a* and A' states, and $|\Delta\Phi|_{\text{av}}$ decreases. After 1 ps, transitions to the *A* and *X* states begin, and on these states asymmetric solvent configurations are favored. Rather than increasing, $|\Delta\Phi|_{\text{av}}$ levels off, reflecting the fact that much of the solvent has evaporated from the cluster. After 5 ps the two spin-orbit relaxed products differ: the dissociative products maintain a steady value of the solvent coordinate, while the solvent coordinate of the recombined products decreases. I_2^- vibrationally relaxes on the *X* state by evaporating CO_2 molecules from the cluster, and for $n=13$ all of the solvent is gone by 20 ps, forcing $\Delta\Phi$ to zero.

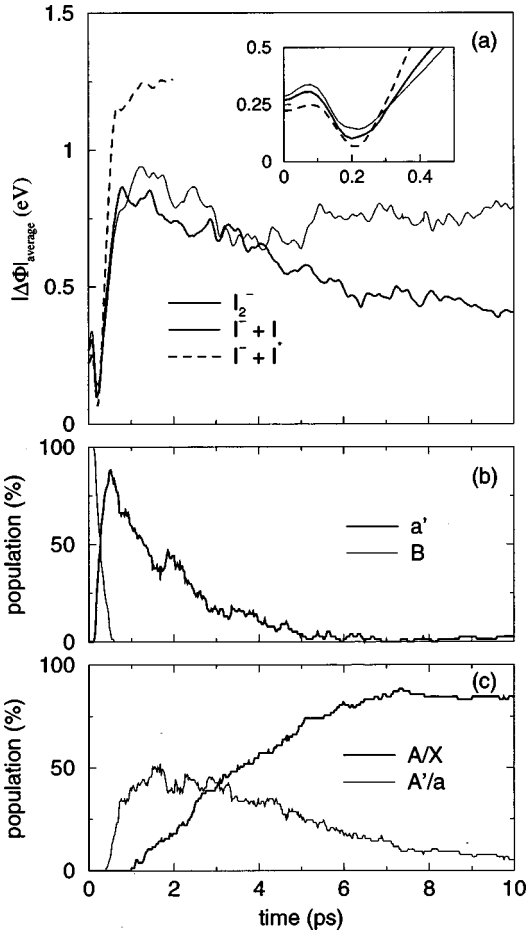

FIG. 9. Properties of the $n=13$ ensemble. (a) Average magnitude of the solvent coordinate vs time, sorted by product channel. (b) and (c) Electronic state populations vs time for trajectories that undergo spin-orbit relaxation. See Sec. IV C for further details.

D. Summary

In Fig. 10 we revisit our qualitative picture of the potential energy of solvated I_2^- and include snapshots of trajectories to summarize the key features of the photodissociation dynamics. Within 200 fs after excitation to the *B* state, the I_2^- bond length is large enough that the energy curves in this schematic diagram apply. The electronic character of state *B*, which localizes the charge on the unsolvated iodine atom, prevents further dissociation. Solvent reorganization toward a symmetric cluster configuration brings about transitions to the a' state. Trajectories that undergo charge transfer predominantly dissociate to solvated $I^- + I^*$ products within

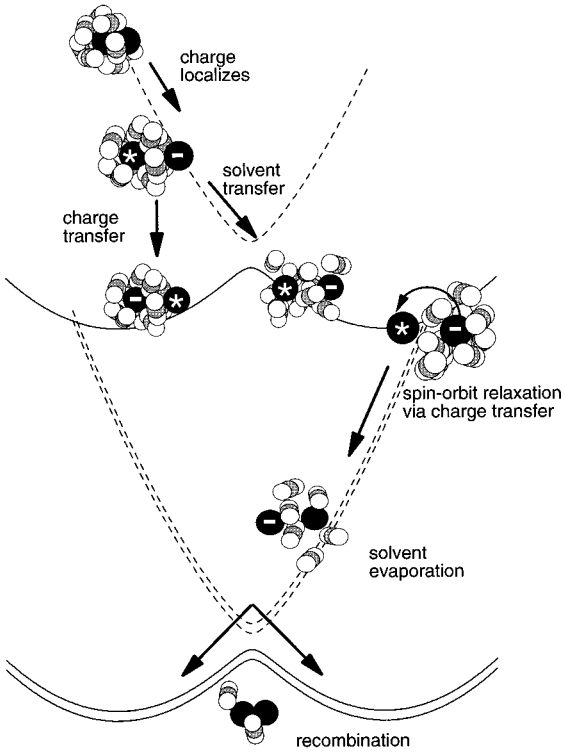

FIG. 10. A summary of the dynamics following 395 nm photoexcitation. The schematic potential energy curves are those of Fig. 4, right-hand panel.

1–5 ps, while trajectories that undergo solvent transfer become trapped temporarily on the a' state. Small clusters remain trapped until I_2^- dissociates by evaporation of I*. For clusters with nine or more CO_2 molecules, however, the asymmetry of the solvent distribution about I_2^- can be large enough to overcome the atomic iodine spin-orbit splitting energy that separates the a' state from the a and A' states. In these systems, we see a strong correlation between solvent transfer during the B to a' transition and subsequent return to the lower spin-orbit manifold. It appears that the early partitioning of energy into solvent motion enhances the likelihood that clusters will reach the large $|\Delta\Phi|$ required to make a nonadiabatic transition to the lower spin-orbit states before the solute bond length becomes too large for the charge transfer that accompanies that transition to occur.

From the a' state, charge transfer to the a or A' state brings about immediate reorganization of the cluster as the spin-orbit excitation energy is converted into solvent motion. In fact, much of the solvent boils off at this point, and it is even possible for dissociation of I_2^- to occur on these anomalous states. As the solvent coordinate returns to zero during this process of energy dissipation, transitions to the A and X states occur, typically within a few hundred femtoseconds of the transition out of the a' state. From this point, trajectories may continue to dissociate, or they may recombine on the X state of I_2^-.

V. CONCLUSION

The results of these simulations demonstrate that our effective Hamiltonian model adequately describes the overall trends in the experimental product branching ratio and the mass distribution of photofragments. While the quantitative agreement between theory and experiment is not as good as in our previous simulations of 790 nm dissociation,[43] the principal new feature seen in UV photodissociation—the onset of extensive spin-orbit quenching in the larger clusters—is well reproduced. In fact, the first indications that spin-orbit quenching could be efficient in these clusters came from the simulations, which preceded the experiments by several months. While the time scales for these processes have not yet been determined experimentally in the CO_2 clusters, the recombination time in OCS clusters is estimated to be on the order of a few picoseconds,[51] consistent with our results.

Our results reinforce the lessons we have learned from previous work. A proper interpretation of the experiments and simulations requires an understanding of the interplay between the solute charge distribution and the solvent environment. These interactions depend strongly on the various electronic states of the solute as well as on the dissociation coordinate, R_{solute}, and thus interpretations based solely on the isolated solute potential curves can be misleading. Just as we found for 790 nm excitation to the A' state, the anomalous charge flow character of the B state prevents dissociation when strong solute-solvent interactions are present. A nonadiabatic transition to a state exhibiting normal charge flow is necessary for dissociation to continue. Strong interactions with the solvent also affect dynamics on normal charge flow states by creating a competition between solvation and chemical bonding, as evidenced by the trapping of trajectories on the a' state. This too parallels behavior observed in the near-IR studies, but there is one important distinction between transient trapping on the a' and A states. To leave the A state, the solute bond length must increase well beyond the equilibrium value, but on the a' state I_2^- can electronically relax via solvent-mediated charge transfer, providing that the solvation energy is greater than the spin-orbit splitting. This relaxation occurs at the shorter solute bond lengths characteristic of the trapped clusters, and the requisite solvent coordinate is readily attained in clusters with more than half a solvation shell of CO_2. Therefore, both electronic relaxation (spin-orbit quenching) and thermal evaporation of neutral iodine deplete the number of clusters trapped on the a' state. The two processes occur on comparable time scales in our simulations; however, electronic relaxation becomes more efficient as cluster size increases.

Analysis of the simulation trajectories using an extension of the electron-transfer picture described in our earlier work strongly suggests that the observed electronic relaxation occurs via charge transfer from solvated I^- to I*, this process being made resonant, and thereby efficient, by reorganization of the solvent following the initial UV excitation. The charge-transfer event converts electronic energy into solvent potential energy, which is dissipated by further solvent rearrangement and evaporation. As a result, the spin-orbit excitation energy is efficiently quenched within the cluster. This mechanism provides an appealing explanation for the sharp onset of spin-orbit quenching with increasing cluster size observed in both simulations and experiments.

ACKNOWLEDGMENTS

We would like to thank our experimental collaborators Andrei Sanov, Todd Sanford, Sreela Nandi, and Carl Lineberger for their contributions and for many illuminating discussions. This work was supported by the National Science Foundation under Grant No. PHY-9512150, and by the National Center for Supercomputing Applications (NCSA) under Grant No. CHE970015N for computing time on the SGI Power ChallengeArray and the SGI CRAY Origin2000 at the NCSA, University of Illinois at Urbana–Champaign.

APPENDIX: MODEL HAMILTONIAN FOR SPIN-ORBIT QUENCHING BY CHARGE TRANSFER

Electron and exciton transfer in condensed media are commonly described by means of semiempirical one-electron Hamiltonians,[49,50,68] which help to identify the key molecular parameters that determine the reaction rate. We present here a model of this type that is suitable for describing the interplay between charge transfer and spin-orbit coupling in solvated dihalide ions. This model provides a Hamiltonian to go along with the qualitative potential curves sketched in Fig. 4, and provides further insight into the mechanism of solvent-induced spin-orbit quenching.

We begin by reviewing the traditional spin-boson Hamiltonian for a two-level electronic system coupled linearly to a single coordinate representing the nuclear degrees of freedom.[50,68,69] In solution-phase electron transfer this coordinate is usually the solvent orientational polarization,[48,49] while in solid-state electron or exciton transfer it may include both lattice and intramolecular vibrations;[50,68] in our clusters, it describes the overall motion of the solvent cage from one side of the solute to the other. We will primarily use the language of solution-phase electron transfer in our discussion. We adopt a diabatic representation in which the basis states describe an electron localized on either of two atoms, labeled A and B, having local site energies ϵ_A and ϵ_B. The model Hamiltonian then takes the form

$$\mathsf{H}=\begin{bmatrix}\epsilon_A & \beta\\ \beta & \epsilon_B\end{bmatrix}+\left(\frac{p^2}{2m}+u(q)\right)\begin{bmatrix}1 & 0\\ 0 & 1\end{bmatrix}+\begin{bmatrix}-\gamma q & 0\\ 0 & \gamma q\end{bmatrix}, \quad \text{(A1)}$$

where β is the electronic resonance integral that parametrizes the chemical bonding interaction between the two sites, q and p are the solvent coordinate and its corresponding momentum, $u(q)$ is the potential energy associated with deforming the solvent configuration, and γ measures the strength of the coupling between the electronic and solvent degrees of freedom. (The product $2\gamma q$, which measures the energy gained by localizing the charge on one site and deforming the solvent around that site, corresponds to the ''solvent coordinate'' $\Delta\Phi$ used in the main text of this paper.) Equation (A1) can be rewritten as the sum of an adiabatic electronic Hamiltonian H^{el} and a solvent kinetic energy term T,

$$\mathsf{H}=\begin{bmatrix}\epsilon_A+u(q)-\gamma q & \beta\\ \beta & \epsilon_B+u(q)+\gamma q\end{bmatrix}+\left(\frac{p^2}{2m}\right)\begin{bmatrix}1 & 0\\ 0 & 1\end{bmatrix}$$
$$\equiv \mathsf{H}^{\mathrm{el}}+\mathsf{T}. \quad \text{(A2)}$$

The diagonal elements of H^{el}, considered as functions of q, trace out the diabatic potential curves, while the eigenvalues of H^{el} yield the corresponding adiabatic curves. If the solvent coordinate is treated as an harmonic oscillator, $u(q)$ is quadratic and the diabatic curves are a pair of displaced parabolas. The resonance coupling β depends strongly (typically exponentially) upon the interatomic separation R. The diabatic representation is most useful at large R, where β is small; in this regime an electronic transition between the diabatic states can be viewed as a charge-transfer event. These transitions occur primarily where the diabatic curves cross, $\epsilon_A-\epsilon_B=2\gamma q$, with a probability proportional to $|\beta|^2$. For a homonuclear diatomic solute, $\epsilon_A=\epsilon_B$ and the diabatic curves cross at $q=0$.

The Hamiltonian above describes a single electron in a state space that includes one orbital per site. Since the dihalide ions are one electron short of a closed shell, their electronic structure can be described in terms of a single-hole picture which is isomorphic to a one-electron picture; however, the state space must be expanded to include the three valence p-orbitals on each atom. We then have two resonance integrals, β_Σ and β_Π, which correspond to chemical bonding interactions between p-orbitals that are respectively parallel and perpendicular to the internuclear axis. For the time being we neglect spin-orbit coupling. In the localized diabatic representation, the six-state adiabatic electronic Hamiltonian consists of three 2×2 blocks, two of which are degenerate,

$$\begin{bmatrix}
\epsilon_A+u(q)-\gamma q & \beta_\Sigma & & & & \\
\beta_\Sigma & \epsilon_B+u(q)+\gamma q & & & & \\
 & & \epsilon_A+u(q)-\gamma q & -\beta_\Pi & & \\
 & & -\beta_\Pi & \epsilon_B+u(q)+\gamma q & & \\
 & & & & \epsilon_A+u(q)-\gamma q & -\beta_\Pi \\
 & & & & -\beta_\Pi & \epsilon_B+u(q)+\gamma q
\end{bmatrix}. \quad \text{(A3)}$$

The signs of the off-diagonal elements have been chosen so that when β_Σ and β_Π are positive, the sigma-bonding state will have ungerade (u) symmetry while the pi-bonding states will have g-symmetry, as in the actual molecule.

The spin-orbit coupling operator $\zeta \mathbf{l}\cdot\mathbf{s}$ mixes the Σ and Π blocks. Because the model Hamiltonian has cylindrical symmetry, we may choose linear combinations within the Π subspace so that only one pair couples to the Σ states; these are the states with a total angular momentum projection $\Omega = 1/2$. The $\Omega = 3/2$ states remain pure Π states and we leave them out. The resulting four-state electronic Hamiltonian is

$$\mathsf{H}^{a}=\begin{bmatrix} \epsilon_A+u(q)-\gamma q & \beta_\Sigma & -\frac{\zeta}{\sqrt{2}} & 0 \\ \beta_\Sigma & \epsilon_B+u(q)+\gamma q & 0 & -\frac{\zeta}{\sqrt{2}} \\ -\frac{\zeta}{\sqrt{2}} & 0 & \epsilon_A+u(q)-\gamma q+\frac{\zeta}{2} & -\beta_\Pi \\ 0 & -\frac{\zeta}{\sqrt{2}} & -\beta_\Pi & \epsilon_B+u(q)+\gamma q+\frac{\zeta}{2} \end{bmatrix}. \tag{A4}$$

We now transform this Hamiltonian from the Hund's Case (a) representation, in which the spin-orbit terms couple basis states that are purely Σ or Π in character, to the Hund's Case (c) representation in which the spin-orbit terms appear on the diagonal. Case (c) is appropriate when the spin-orbit splitting exceeds the resonance coupling, as is always the case at sufficiently large interatomic distances; for isolated I_2^- the electronic wave functions are well described in Hund's Case (c) for R greater than about 6 Å.[55] Since the transformation mixes Σ and Π states, one ends up with localized basis states that interact through linear combinations of β_Σ and β_Π,

$$\mathsf{H}^{c}=\begin{bmatrix} \epsilon_A+u(q)-\gamma q+\zeta & \frac{1}{3}(\beta_\Sigma-2\beta_\Pi) & 0 & \frac{\sqrt{2}}{3}(\beta_\Sigma+\beta_\Pi) \\ \frac{1}{3}(\beta_\Sigma-2\beta_\Pi) & \epsilon_B+u(q)+\gamma q+\zeta & \frac{\sqrt{2}}{3}(\beta_\Sigma+\beta_\Pi) & 0 \\ 0 & \frac{\sqrt{2}}{3}(\beta_\Sigma+\beta_\Pi) & \epsilon_A+u(q)-\gamma q-\frac{1}{2}\zeta & \frac{1}{3}(2\beta_\Sigma-\beta_\Pi) \\ \frac{\sqrt{2}}{3}(\beta_\Sigma+\beta_\Pi) & 0 & \frac{1}{3}(2\beta_\Sigma-\beta_\Pi) & \epsilon_B+u(q)+\gamma q-\frac{1}{2}\zeta \end{bmatrix}. \tag{A5}$$

The upper 2×2 block of H^c describes the resonance interaction between an I^- ion and an I* atom, and the lower to the interaction between I^- and I in its spin-orbit ground state. Indeed, one can think of the linear combinations of β_Σ and β_Π as arising from p-orbitals that are tilted away from the internuclear axis by 30 and 60 deg. The diagonal elements of H^c, considered as functions of q, correspond to the diabatic potential curves in Fig. 4 (although Fig. 4 also includes the $\Pi_{3/2}$ states that have been omitted here). Within each spin-orbit block, charge transfer occurs primarily near $q=0$ where the diabatic curves cross. However, Eq. (A5) also includes matrix elements $(\sqrt{2}/3)(\beta_\Sigma+\beta_\Pi)$ that couple the spin-orbit blocks. Since these matrix elements are made up from interatomic resonance integrals, they also describe charge-transfer events, and they will become important when the diabatic curves arising from *different* spin-orbit blocks cross, as in Fig. 4. In the homonuclear case ($\epsilon_A = \epsilon_B$) the condition for such a crossing is that

$$\tfrac{3}{2}\zeta = \pm 2\gamma q \equiv \Delta\Phi, \tag{A6}$$

i.e., the differential solvation energy is equal to the spin-orbit splitting in the iodine atom. Thus, these are the matrix elements responsible for spin-orbit relaxation via solvent-induced charge transfer.

At a given R, we expect that β_Σ will be much larger than β_Π since a p-orbital hole that is aligned with the internuclear axis will have a larger overlap with the charge cloud on the I^- ion than one which is aligned perpendicular to that axis. This expectation is confirmed by the relative depths of the Σ and Π state wells in I_2^-: the ground state ($^2\Sigma_{u,1/2}$) is bound by 1.01 eV[10] while the binding energy in the first excited state ($^2\Pi_{g,1/2}$) is estimated to be about 0.1 eV.[55] To a first approximation, we may regard all the charge-transfer events

as driven by β_Σ, whose amplitude is distributed in varying amounts over the spin-orbit coupled Hund's Case (c) states. All of the charge-transfer matrix elements in H^c are then of the same order of magnitude; if anything, the terms associated with charge transfer between the two spin-orbit manifolds are somewhat larger than those associated with charge transfer in the spin-orbit excited state. Thus there are no matrix-element restrictions on spin-orbit relaxation by charge transfer: the electron hops to whichever orbital is closest in energy. When the two atoms are equally solvated ($q \approx 0$), the charge is transferred within a spin-orbit manifold, but in a highly asymmetric solvent environment ($2\gamma q \approx \pm(3/2)\zeta$), charge transfer involves a transition between the spin-orbit manifolds.

The model outlined above has one significant unphysical property: the Hamiltonian is cylindrically symmetric. This is a result of compressing the solvent effects into a single coordinate that describes only the overall difference between the solvation energies at the two atoms, not the finer details of the complicated electrostatic environment around the solute. When these details are included, as they are in our simulations, Ω is no longer a good quantum number and the electronic Hamiltonian cannot be reduced to four states. As a result, the spin-orbit excited states are quenched into all four lower states, rather than into one pair as in the model above. This is seen in the simulations. Aside from this, the Hamiltonian model describes well the overall features of the solvent-mediated spin-orbit quenching mechanism: the process does not occur at all until a threshold value of the solvent coordinate is reached, but once this criterion is met the process is highly efficient.

[1] M. Alexander, N. Levinger, M. Johnson, D. Ray, and W. C. Lineberger, J. Chem. Phys. **88**, 6200 (1988).
[2] D. Ray, N. Levinger, J. Papanikolas, and W. C. Lineberger, J. Chem. Phys. **91**, 6533 (1989).
[3] J. Papanikolas, J. Gord, N. Levinger, D. Ray, V. Vorsa, and W. C. Lineberger, J. Phys. Chem. **95**, 8028 (1991).
[4] J. Papanikolas, V. Vorsa, M. Nadal, P. Campagnola, J. Gord, and W. C. Lineberger, J. Chem. Phys. **97**, 7002 (1992).
[5] J. Papanikolas, V. Vorsa, M. Nadal, P. Campagnola, H. Buchenau, and W. C. Lineberger, J. Chem. Phys. **99**, 8733 (1993).
[6] V. Vorsa, S. Nandi, P. J. Campagnola, M. Larsson, and W. C. Lineberger, J. Chem. Phys. **106**, 1402 (1997).
[7] S. Nandi, A. Sanov, N. Delaney, J. Faeder, R. Parson, and W. C. Lineberger, J. Phys. Chem. A **102**, 8827 (1998).
[8] B. J. Greenblatt, M. T. Zanni, and D. M. Neumark, Chem. Phys. Lett. **258**, 523 (1996).
[9] B. J. Greenblatt, M. T. Zanni, and D. M. Neumark, Science **276**, 1675 (1997).
[10] M. T. Zanni, T. R. Taylor, B. J. Greenblatt, B. Soep, and D. M. Neumark, J. Chem. Phys. **107**, 7613 (1997).
[11] B. J. Greenblatt, M. T. Zanni, and D. M. Neumark, Faraday Discuss. **108**, 101 (1997).
[12] K. R. Asmis, T. R. Taylor, C. S. Xu, and D. M. Neumark, J. Chem. Phys. **109**, 4389 (1998).
[13] A. E. Johnson, N. E. Levinger, and P. F. Barbara, J. Phys. Chem. **96**, 7841 (1992).
[14] J. Alfano, Y. Kimura, P. K. Walhout, and P. F. Barbara, Chem. Phys. **175**, 147 (1993).
[15] D. A. V. Kliner, J. C. Alfano, and P. F. Barbara, J. Chem. Phys. **98**, 5375 (1993).
[16] P. K. Walhout, J. C. Alfano, K. A. M. Thakur, and P. F. Barbara, J. Phys. Chem. **99**, 7568 (1995).
[17] U. Banin, A. Waldman, and S. Ruhman, J. Chem. Phys. **96**, 2416 (1992).
[18] U. Banin and S. Ruhman, J. Chem. Phys. **98**, 4391 (1993).
[19] U. Banin and S. Ruhman, J. Chem. Phys. **99**, 9318 (1993).
[20] U. Banin, R. Kosloff, and S. Ruhman, Chem. Phys. **183**, 289 (1994).
[21] E. Gershgoren, U. Banin, and S. Ruhman, J. Phys. Chem. A **102**, 9 (1998).
[22] H. Yasumatsu, S. Koizumi, A. Terasaki, and T. Kondow, J. Chem. Phys. **105**, 9509 (1996).
[23] H. Yasumatsu, A. Terasaki, and T. Kondow, J. Chem. Phys. **106**, 3806 (1997).
[24] H. Yasumatsu, U. Kalmbach, S. Koizumi, A. Terasaki, and T. Kondow, Z. Phys. D **40**, 51 (1997).
[25] H. Yasumatsu, S. Koizumi, A. Terasaki, and T. Kondow, J. Phys. Chem. A **102**, 9581 (1998).
[26] L. Perera and F. G. Amar, J. Chem. Phys. **90**, 7354 (1989).
[27] F. G. Amar and L. Perera, Z. Phys. D **20**, 173 (1991).
[28] I. Benjamin and R. M. Whitnell, Chem. Phys. Lett. **204**, 45 (1993).
[29] I. Benjamin, U. Banin, and S. Ruhman, J. Chem. Phys. **98**, 8337 (1993).
[30] U. Banin, A. Bartana, S. Ruhman, and R. Kosloff, J. Chem. Phys. **101**, 8461 (1994).
[31] G. Ashkenazi, U. Banin, A. Bartana, R. Kosloff, and S. Ruhman, Adv. Chem. Phys. **100**, 317 (1997).
[32] B. J. Gertner, K. Ando, R. Bianco, and J. T. Hynes, Chem. Phys. **183**, 309 (1994).
[33] R. Bianco and J. T. Hynes, J. Chem. Phys. **102**, 7864 (1995).
[34] R. Bianco and J. T. Hynes, J. Chem. Phys. **102**, 7885 (1995).
[35] I. Benjamin, P. F. Barbara, B. J. Gertner, and J. T. Hynes, J. Phys. Chem. **99**, 7557 (1995).
[36] P. E. Maslen, J. M. Papanikolas, J. Faeder, R. Parson, and S. V. ONeil, J. Chem. Phys. **101**, 5731 (1994).
[37] J. M. Papanikolas, P. E. Maslen, and R. Parson, J. Chem. Phys. **102**, 2452 (1995).
[38] B. M. Ladanyi and R. Parson, J. Chem. Phys. **107**, 9326 (1997).
[39] J. G. Dojahn, E. C. M. Chen, and W. E. Wentworth, J. Phys. Chem. **100**, 9649 (1996).
[40] E. C. M. Chen, J. G. Dojahn, and W. E. Wentworth, J. Phys. Chem. A **101**, 3088 (1997).
[41] V. S. Batista and D. F. Coker, J. Chem. Phys. **106**, 7102 (1997).
[42] J. Faeder, N. Delaney, P. E. Maslen, and R. Parson, Chem. Phys. Lett. **270**, 196 (1997).
[43] N. Delaney, J. Faeder, P. E. Maslen, and R. Parson, J. Phys. Chem. A **101**, 8147 (1997).
[44] P. E. Maslen, J. Faeder, and R. Parson, Mol. Phys. **94**, 693 (1998).
[45] J. Faeder, N. Delaney, P. E. Maslen, and R. Parson, Chem. Phys. **239**, 525 (1998).
[46] C. Margulis and D. F. Coker, J. Chem. Phys. **110**, 5677 (1999).
[47] J. Faeder and R. Parson, J. Chem. Phys. **108**, 3909 (1998).
[48] R. A. Marcus, Annu. Rev. Phys. Chem. **15**, 155 (1964).
[49] M. D. Newton and N. Sutin, Annu. Rev. Phys. Chem. **35**, 437 (1984).
[50] G. C. Schatz and M. A. Ratner, *Quantum Mechanics in Chemistry* (Prentice Hall, Englewood Cliffs, NJ, 1993), Chap. 10.
[51] A. Sanov, T. Sanford, S. Nandi, and W. C. Lineberger, J. Chem. Phys. **111**, 664 (1999), following paper.
[52] D. Husain and R. J. Donovan, in *Advances in Photochemistry*, edited by J. N. Pitts, Jr., G. S. Hammond, and W. A. Noyes, Jr. (Wiley-Interscience, New York, 1971), Vol. 8, pp. 1–75.
[53] A. V. Benderskii, R. Zadoyan, and V. A. Apkarian, J. Chem. Phys. **107**, 8437 (1997).
[54] R. Zadoyan, M. Sterling, M. Ovchinnikov, and V. A. Apkarian, J. Chem. Phys. **107**, 8446 (1997).
[55] P. E. Maslen, J. Faeder, and R. Parson, Chem. Phys. Lett. **263**, 63 (1996).
[56] C. S. Murthy, S. F. O'Shea, and I. R. McDonald, Mol. Phys. **50**, 531 (1983).
[57] C. G. Gray and K. E. Gubbins, *Theory of Molecular Fluids* (Clarendon, Oxford, 1984), Vol. 1.
[58] A. J. Stone, *The Theory of Intermolecular Forces* (Oxford, New York, 1996).
[59] Y. Zhao, C. C. Arnold, and D. M. Neumark, J. Chem. Soc., Faraday Trans. **89**, 1449 (1993).
[60] H. C. Andersen, J. Comput. Phys. **52**, 24 (1982).
[61] J. C. Tully, J. Chem. Phys. **93**, 1061 (1990).
[62] S. Hammes-Schiffer and J. C. Tully, J. Chem. Phys. **101**, 4657 (1994).
[63] J. M. Papanikolas, Ph.D. thesis, University of Colorado, 1994.
[64] V. Vorsa, P. J. Campagnola, S. Nandi, M. Larsson, and W. C. Lineberger, J. Chem. Phys. **105**, 2298 (1996).
[65] These are not, strictly speaking, true adiabatic curves because they cross at a large solvent coordinate. In the true adiabats these crossings would be

avoided. The curves in Fig. 4 correspond instead to an intermediate representation which exactly diagonalizes the electronic Hamiltonian only at $\Delta\Phi=0$. This is more convenient than the true adiabatic representation, which diagonalizes the electronic Hamiltonian for all $\Delta\Phi$, because the curves can be labeled with the molecular state labels of isolated I_2^-.

[66] It is possible, but rarely observed in the simulations ($<1\%$ of trajectories), for direct dissociation on the *B* state to occur, producing a light I^- fragment and solvated I*, analogous to the A' state, low mass dissociative products reported for $I_2^-Ar_n$ clusters (Ref. 6).

[67] B. J. Greenblatt, M. T. Zanni, and D. M. Neumark, private communication.

[68] R. J. Silbey, Annu. Rev. Phys. Chem. **27**, 203 (1976).

[69] R. Englman, *The Jahn-Teller Effect in Molecules and Crystals* (Wiley-Interscience, New York, 1972).